Rakenteiden Mekaniikka (Journal of Structural Mechanics)
Vol. 45, No 2, 2012, pp. 59-71

A simple J2-plasticity-damage model for metals in the small strain regime

Timo Saksala

Summary. This article presents a simple constitutive model for metal plasticity. The model is based on the classical small strain J_2-flow theory with nonlinear isotropic and kinematic hardening laws and isotropic damage concept. The introduction of damage extends the capabilities of plain plasticity models to account for the stiffness degradation observed in the experiments. The plastic and damage parts of the model are combined in the effective stress space so that the plasticity computations, i.e. the stress return mapping, can be performed independently of the damage computations. This effective stress space formulation results in a particularly simple formulation of the combined model which enables rather easy derivation of the consistent tangent modulus. The performance of the model is demonstrated with numerical examples using a single (finite) element model.

Key words: J_2-flow theory, isotropic damage, metal plasticity, small strain

Introduction

Metal structures and machine parts have been traditionally designed so that the yield strength of the material is not exceeded, i.e. plastic deformations or damage are not allowed, in any operational conditions. However, considerations involving plasticity and damage are needed, e.g., in collapse analyses of steel frames and low-cycle fatigue analyses of machine components. Ductile damage of metals occurs simultaneously with plastic deformation larger than certain threshold. Therefore, a material model aiming at realistic prediction of failure conditions should accommodate both the damage and plasticity descriptions.

J_2-flow theory, i.e. an elastoplastic model based on the von Mises yield function with associated flow rule, is the most popular model in computational plasticity analyses of metals. During the last five decades, the model has been extended from its classical form characterizing the material with elastic-perfectly plastic or isotropic hardening behavior to complex behavior of various materials including nonlinear isotropic and/or kinematic hardening, anisotropy, strain rate dependency and damage [1][2][3]. By introduction of the damage concept into the classical J_2-plasticity model, it can accommodate the stiffness and strength degradation, as illustrated schematically in Figure 1b, resulting from the breakage of atomic bonds due to an accumulation of arrested dislocations [1].

The classical J_2-plasticity model with the linear hardening model implemented in FEM and Newton-Raphson algorithm to solve the discretised equilibrium equations can

predict the material response up to the point at which the slope of the stress-strain curve reaches zero, i.e. the turning point from hardening to softening (see Figure 1a). The softening regime can, of course, be modelled with a softening plasticity model and a path following algorithm. It seems simpler, however, to enhance the classical model by combining it with a damage model since then no softening plasticity model is needed and the stiffness degradation can be accounted for at the same computational cost.

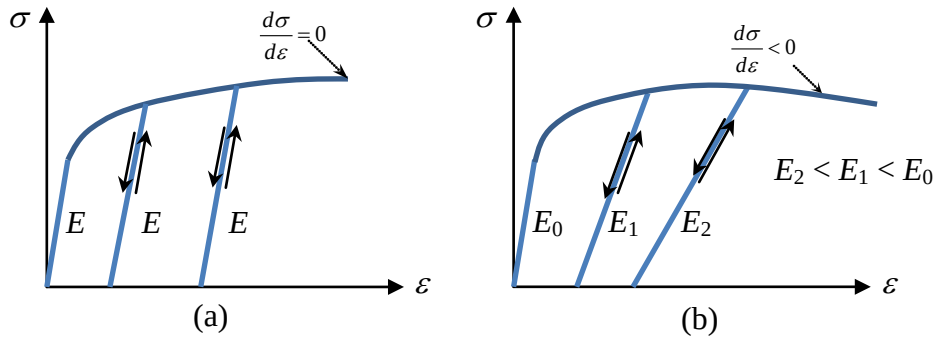

Figure 1. Schematic 1D illustration of the material response in uniaxial tension with a classical hardening plasticity model (a) and a plasticity-damage model (b).

The purpose of this paper is to present a simple extension of the classical model equipped with nonlinear kinematic and isotropic hardening laws to account for the stiffness and strength degradation via isotropic damage concept. The model is formulated under the small deformation (strains and rotations) framework. The damage and plasticity parts of the model are combined with the effective stress space formulation which allows for a separate treatment of the plasticity and damage computations and results in a particularly simple consistent tangent matrix. The theory is illustrated with numerical examples using a single element model, i.e. only constitutive response of the model is demonstrated.

Theory of the model

Classical J_2 plasticity with nonlinear isotropic and kinematic hardening

For present purposes the yield function of J_2-plasticity, i.e. the von Mises criterion, is defined as follows

$$\begin{aligned} f_{\mathrm{vM}}(\boldsymbol{\xi}, R) &= \sqrt{J_2} - (\sigma_Y + R) \\ J_2 &= \tfrac{1}{2}\mathrm{dev}(\boldsymbol{\xi}) : \mathrm{dev}(\boldsymbol{\xi}) \\ \boldsymbol{\xi} &= \boldsymbol{\sigma} - \mathbf{X} \end{aligned} \tag{1}$$

where $\mathrm{dev}(\boldsymbol{\xi}) = \boldsymbol{\xi} - \frac{1}{3}\mathrm{tr}(\boldsymbol{\xi})\mathbf{I}$ ($\mathbf{I}$ being the second order identity tensor) is the deviator, σ_Y is the yield strength, $\boldsymbol{\sigma}$ is the stress tensor, $\mathbf{X}$ is the so-called back stress tensor related to kinematic hardening, and R is the isotropic hardening variable. Following Lemaitre [1],

the hardening functions for both the isotropic and kinematic hardening are assumed to be nonlinear in equivalent plastic strain by

$$\begin{aligned} R &= R_\infty \left(1 - \exp(-b\varepsilon^p_{\text{eqv}})\right) \\ \mathbf{X} &= X_\infty \left(1 - \exp(-\gamma\varepsilon^p_{\text{eqv}})\right)\frac{\partial f_{\text{vM}}}{\partial \boldsymbol{\sigma}} \end{aligned} \tag{2}$$

where R_∞ and X_∞ are saturation stresses of the isotropic and kinematic hardening, respectively, b and γ are hardening parameters to be determined from the experiments, and $\varepsilon^p_{\text{eqv}}$ is the equivalent plastic strain defined via its rate as

$$\dot{\varepsilon}^p_{\text{eqv}} = \sqrt{\tfrac{2}{3}\dot{\boldsymbol{\varepsilon}}^p : \dot{\boldsymbol{\varepsilon}}^p} \tag{3}$$

with $\boldsymbol{\varepsilon}^p$ being the plastic strain tensor.

The underlying assumption in the small strain plasticity framework is the additive split of the total strain into the elastic and plastic parts:

$$\dot{\boldsymbol{\varepsilon}} = \dot{\boldsymbol{\varepsilon}}^e + \dot{\boldsymbol{\varepsilon}}^p \tag{4}$$

The rate of the plastic strain in (4) is defined via the associative flow rule as

$$\dot{\boldsymbol{\varepsilon}}^p = \dot{\lambda}\frac{\partial f_{\text{vM}}}{\partial \boldsymbol{\sigma}} = \dot{\lambda}\frac{\text{dev}(\boldsymbol{\xi})}{\sqrt{J_2}} \tag{5}$$

where $\dot{\lambda}$ is the plastic increment.

With relations (3) and (5) the hardening evolution laws can now be derived as the time derivatives of the hardening functions (2). Accordingly, by the chain rule,

$$\begin{aligned} \dot{R} &= R_\infty b \exp(-b\varepsilon^p_{\text{eqv}})\dot{\lambda}\sqrt{\tfrac{2}{3}\partial_{\boldsymbol{\sigma}} f_{\text{vM}} : \partial_{\boldsymbol{\sigma}} f_{\text{vM}}} = h_R(\xi, \varepsilon^p_{\text{eqv}})\dot{\lambda} \\ \dot{\mathbf{X}} &= X_\infty \gamma \exp(-\gamma\varepsilon^p_{\text{eqv}})\dot{\lambda}\sqrt{\tfrac{2}{3}\partial_{\boldsymbol{\sigma}} f_{\text{vM}} : \partial_{\boldsymbol{\sigma}} f_{\text{vM}}}\partial_{\boldsymbol{\sigma}} f_{\text{vM}} = h_X(\xi, \varepsilon^p_{\text{eqv}})\dot{\lambda}\partial_{\boldsymbol{\sigma}} f_{\text{vM}} \end{aligned} \tag{6}$$

where symbol $\partial_{\mathbf{x}}$ denotes derivation with respect to $\mathbf{x}$ (here tensor). In view of the flow rule (5), it is observed from Equation (6) that the back stress is proportional to the plastic strain. In order to complete the model from the computational point of view, it is noted that, along with the above equations, consistency conditions of Kuhn-Tucker form

$$f_{\text{vM}} \le 0, \quad \dot{\lambda} \ge 0, \quad \dot{\lambda} f_{\text{vM}} = 0, \quad \dot{\lambda}\dot{f}_{\text{vM}} = 0 \tag{7}$$

must be fulfilled. The hardening functions defined in (2) are more realistic than the usually employed linear hardening rules since it is experimentally observed that both hardening types tend to saturate [1]. Next, the damage part of the model is presented.

Isotropic damage concept

At the micro-scale, the mechanism of damage is debonding and microcracking thereof. At the meso-scale damage can, however, manifest as brittle, ductile and creep damage depending on the loading conditions, temperature and the nature of the material. In this paper only ductile damage of metals is considered. For a detailed account of different damage mechanisms, see Lemaitre [1].

Since metals can be treated as isotropic and homogeneous materials, the damage is assumed isotropic in this paper. This more or less justified assumption implies that the effect of damage on the constitutive equations can be treated with a scalar damage variable ω that relates, in 1D case, the effective cross-sectional area, A_{eff}, of a bar in tension to its initial or nominal area A_0, as $\omega = 1 - A_{\text{eff}}/A_0$. The basic components of a scalar damage model are the nominal-effective stress relation

$$\boldsymbol{\sigma} = (1-\omega)\overline{\boldsymbol{\sigma}} \tag{8}$$

and

$$\begin{aligned} &f_{\text{d}}(\boldsymbol{\varepsilon}, \kappa_{\text{d}}) = \tilde{\varepsilon}(\boldsymbol{\varepsilon}) - \kappa_{\text{d}} \\ &\omega = g_{\text{d}}(\kappa_{\text{d}}) \\ &f_{\text{d}} \le 0,\ \dot{\kappa}_{\text{d}} \ge 0,\ \dot{\kappa}_{\text{d}} f_{\text{d}} = 0 \end{aligned} \tag{9}$$

where f_{d} is the damage loading function, $\tilde{\varepsilon}$ is the equivalent strain, κ_{d} is the damage-driving variable, and g_{d} is the damage evolution function. The damage loading function defines the elastic domain, i.e. the set of stress states where no damage growth occurs. The equivalent strain accounts for the multiaxiality of the strain state.

As ductile damage of metals is modeled in this paper, the damage process is driven by the plastic strain, i.e. $\kappa_{\text{d}} = \varepsilon^p_{\text{eqv}}$. Therefore, no damage function is needed since the von Mises yield criterion indicates stress states resulting in plastic flow and hence the damage evolution as well.

A very simple linear damage evolution function is chosen as

$$\omega = g_{\text{d}}(\varepsilon^p_{\text{eqv}}) = \begin{cases} 0, \text{ if } \varepsilon^p_{\text{eqv}} < \varepsilon_{\text{pD}} \\ \omega_c \dfrac{\varepsilon^p_{\text{eqv}} - \varepsilon_{\text{pD}}}{\varepsilon_{\text{pR}} - \varepsilon_{\text{pD}}}, \text{ if } \varepsilon_{\text{pD}} \le \varepsilon^p_{\text{eqv}} < \varepsilon_{\text{pR}} \\ \omega_c, \text{ if } \varepsilon^p_{\text{eqv}} \ge \varepsilon_{\text{pR}} \end{cases} \tag{10}$$

where ε_{pD} and ε_{pR} are the damage threshold and rupture strain, respectively, and ω_c is the critical value of damage leading to rupture.

As the damage variable is related to the degrading effect of an opening microcrack or microcavity in tension, relation (8) may not be valid in compression. In compression microcracks tend to close and thus the stiffness of the material is recovered. This effect can be treated easily with the Heaviside function in 1D case but the multiaxial case is far from trivial. Following Lemaitre [1], the decomposition of the principal stress in the positive and negative parts can be employed. Accordingly,

$$\begin{aligned} &\boldsymbol{\sigma} = (1-\omega)\overline{\boldsymbol{\sigma}}_+ + (1-h\omega)\overline{\boldsymbol{\sigma}}_- \quad (\overline{\boldsymbol{\sigma}} = \overline{\boldsymbol{\sigma}}_+ + \overline{\boldsymbol{\sigma}}_-) \\ &\overline{\boldsymbol{\sigma}}_+ = \sum_{i=1}^{3} \langle \overline{\sigma}_i \rangle \mathbf{n}_i \otimes \mathbf{n}_i,\ \overline{\boldsymbol{\sigma}}_- = \sum_{i=1}^{3} \langle -\overline{\sigma}_i \rangle \mathbf{n}_i \otimes \mathbf{n}_i \end{aligned} \tag{11}$$

where <> denote the McAuley brackets, $\overline{\sigma}_i$ and $\mathbf{n}_i$ are the principal stress and corresponding direction of the effective stress, and h is a crack closure parameter.

According to Lemaitre [1] this parameter is usually of the same magnitude as ω_c. Next, the plasticity and damage parts of the model are combined.

Combining the plasticity and damage parts of the model

The plasticity and damage parts of the model are combined with the effective stress space formulation. It provides a natural means to separate the plasticity and damage computations so that the robust methods of computational plasticity can be employed in the stress integration [4].

According to this method, an effective stress state violating the yield criterion is first returned onto the yield surface with the stress return scheme chosen and then the damage variable is updated (Equation (10)) and the nominal stress is calculated according to Equation (8) or (11) in cyclic loading. Next, the stress return mapping is presented.

Stress return scheme

The stress return scheme for the classical J_2-plasticity model with linear hardening law is particularly simple due to the existence of an exact solution via the radial return mapping. With the present model iteration is needed due to the nonlinearity of the hardening laws. In this section a stress integration algorithm and a consistent tangent stiffness matrix for the combined model are presented.

Return mapping algorithm

The stress return is performed with the generalised cutting plane algorithm illustrated geometrically in Figure 2. This method is an explicit procedure that involves only functional evaluations and has a quadratic convergence rate in state variables [3].

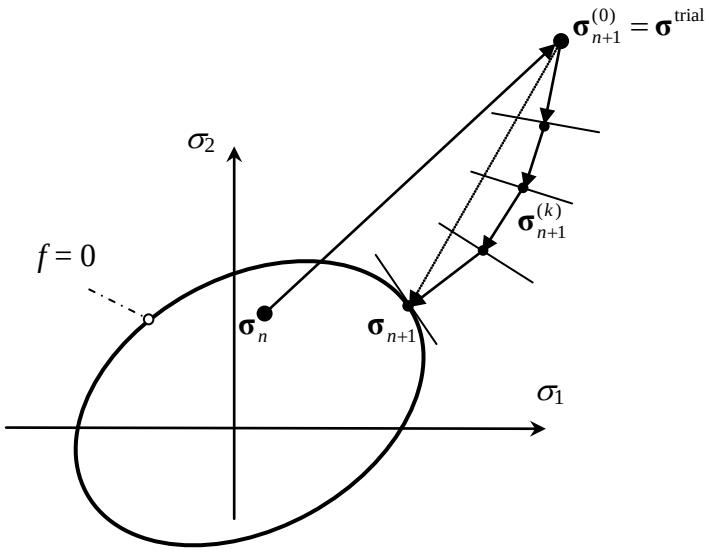

Figure 2. Geometric illustration of the cutting plane algorithm in 2D principal stress space.

The method is based on the usual elastic predictor-plastic corrector splitting. A trial stress state violating the yield surface is returned on this surface iteratively. At each iterate $(\bullet)^{(k)}$ the constraint

$$\begin{aligned} &\text{Find } \Delta\lambda \text{ such that} \\ &f(\Delta\lambda) := f\big(\boldsymbol{\sigma}(\Delta\lambda), \mathbf{q}(\Delta\lambda)\big) = 0 \end{aligned} \tag{12}$$

is linearized. In Equation (12), $\Delta\lambda$ is the plastic increment and $\mathbf{q}$ is a vector of internal variables. The next iterate $(\bullet)^{(k+1)}$ is determined as the intersection of the plane normal to $f^{(k)} = 0$ with the level set $f^{(k+1)}$ [3].

The main steps of the algorithm applied to the present model are:

Trial elastic predictor

Given: $\boldsymbol{\varepsilon}_{n+1}, \boldsymbol{\varepsilon}_n^p, \mathbf{X}_n, R_n, \varepsilon_{\text{eqv},n}^p$

Compute the trial state: $\boldsymbol{\sigma}_{n+1}^{\text{trial}} = \mathbf{E} : (\boldsymbol{\varepsilon}_{n+1} - \boldsymbol{\varepsilon}_n^{\text{p}}),\ \xi_{n+1}^{\text{trial}} = \boldsymbol{\sigma}_{n+1}^{\text{trial}} - \mathbf{X}_n,\ f_{\text{vM}}^{\text{trial}} = f_{\text{vM}}(\xi_{n+1}^{\text{trial}}, R_n)$

If $f_{\text{vM}}^{\text{trial}} > 0$ Set : $\boldsymbol{\varepsilon}_{n+1}^{p,(0)} = \boldsymbol{\varepsilon}_n^p,\ \mathbf{X}_{n+1}^0 = \mathbf{X}_n,\ \boldsymbol{\sigma}_{n+1}^0 = \boldsymbol{\sigma}_{n+1}^{\text{trial}},\ R_{n+1}^0 = R_n,\ \varepsilon_{\text{eqv},n+1}^{p,(0)} = \varepsilon_{\text{eqv},n}^p,\ k = 0$ and perform *plastic corrector*. Else, trial state is correct.

Plastic corrector

1. $\Delta\lambda = \dfrac{f_{\text{vM}}(\xi_{n+1}^k, R_{n+1}^k)}{\partial_{\boldsymbol{\sigma}} f_{\text{vM}} : \mathbf{E} : \partial_{\boldsymbol{\sigma}} f_{\text{vM}} + h_R(\xi_{n+1}^k, \varepsilon_{\text{eqv},n+1}^{p,(k)}) + h_X(\xi_{n+1}^k, \varepsilon_{\text{eqv},n+1}^{p,(k)}) \partial_{\boldsymbol{\sigma}} f_{\text{vM}} : \partial_{\boldsymbol{\sigma}} f_{\text{vM}}}$
2. $\Delta\boldsymbol{\varepsilon}^p = \Delta\lambda \dfrac{\partial f_{\text{vM}}(\xi_{n+1}^k, R_{n+1}^k)}{\partial \boldsymbol{\sigma}}$
3. $R_{n+1}^{k+1} = R_{n+1}^k + h_R(\xi_{n+1}^k, \varepsilon_{\text{eqv},n+1}^{p,(k)})\Delta\lambda$
4. $\mathbf{X}_{n+1}^{k+1} = \mathbf{X}_{n+1}^k + h_X(\xi_{n+1}^k, \varepsilon_{\text{eqv},n+1}^{p,(k)})\Delta\boldsymbol{\varepsilon}^p$
5. $\boldsymbol{\sigma}_{n+1}^{k+1} = \boldsymbol{\sigma}_{n+1}^k - \mathbf{E} : \Delta\boldsymbol{\varepsilon}^p,\ \xi_{n+1}^{k+1} = \boldsymbol{\sigma}_{n+1}^{k+1} - \mathbf{X}_{n+1}^{k+1}$
6. $\boldsymbol{\varepsilon}_{n+1}^{p,(k+1)} = \boldsymbol{\varepsilon}_{n+1}^{p,(k)} + \Delta\boldsymbol{\varepsilon}^p,\ \varepsilon_{\text{eqv},n+1}^{p,(k+1)} = \varepsilon_{\text{eqv},n+1}^{p,(k)} + \sqrt{\tfrac{2}{3}\Delta\boldsymbol{\varepsilon}^p : \Delta\boldsymbol{\varepsilon}^p}$

If $f_{\text{vM}}(\xi_{n+1}^{k+1}, R_{n+1}^{k+1}) \le TOL$ Then exit.

Else set $k \leftarrow k+1$ and go to 1.

In the above algorithm **E** is the linear elasticity tensor. A single-step exact solution exists despite the nonlinearity of the hardening functions (2). This is due to the structure of the plastic corrector according which the hardening moduli in Steps 3 and 4 are evaluated with the equivalent plastic strain from the previous iteration *k*. This feature combined with the fact that an exact (single-step) solution exists for the same model with a linear hardening laws implies the existence of the exact solution. Thus, essentially the cutting plane algorithm for the present J_2-plasticity model results in a piecewise linear approximation of the hardening functions (2).

Consistent tangent modulus

Consistent tangent modulus is needed to speed up the convergence in solving the system equations at the global level with the Newton-Raphson iteration. According to Simo and Hughes [3], the exact linearization of the generalized cutting plane algorithm cannot be obtained in closed form. However, as the exact solution exists for the present J_2-plasticity model with both the cutting plane algorithm and with the general closest point return mapping (which is the radial return mapping in case of J_2-plasticity) in case of linear hardening laws, the consistent tangent modulus of the latter method can be used here as well. It can be written in form (for the derivation, see [3])

$$\mathbf{E}^{\mathrm{epc}} = \mathbf{E}^{\mathrm{c}} - \frac{\mathbf{E}^{\mathrm{c}} : \dfrac{\partial f_{\mathrm{vM}}}{\partial \boldsymbol{\sigma}} \otimes \mathbf{E}^{\mathrm{c}} : \dfrac{\partial f_{\mathrm{vM}}}{\partial \boldsymbol{\sigma}}}{\dfrac{\partial f_{\mathrm{vM}}}{\partial \boldsymbol{\sigma}} : \mathbf{E}^{\mathrm{c}} : \dfrac{\partial f_{\mathrm{vM}}}{\partial \boldsymbol{\sigma}} + h_R + h_X \dfrac{\partial f_{\mathrm{vM}}}{\partial \boldsymbol{\sigma}} : \dfrac{\partial f_{\mathrm{vM}}}{\partial \boldsymbol{\sigma}}} \quad \text{with}$$
$$\mathbf{E}^{\mathrm{c}} = \left(\mathbf{E}^{-1} + \Delta\lambda \frac{\partial^2 f_{\mathrm{vM}}}{\partial \boldsymbol{\sigma}^2} \right)^{-1} \tag{13}$$

This is the consistent elastoplastic tangent modulus with no coupling to damage. In order to account for damage, Equation (8) is perturbed slightly as

$$\begin{aligned} \delta\boldsymbol{\sigma} &= (1-\omega)\delta\overline{\boldsymbol{\sigma}} - \delta\omega\overline{\boldsymbol{\sigma}} \\ &= (1-\omega)\mathbf{E}^{\mathrm{epc}} : \delta\boldsymbol{\varepsilon} - g'_{\mathrm{d}}(\varepsilon^p_{\mathrm{eqv}})\overline{\boldsymbol{\sigma}} \otimes \frac{\partial \varepsilon^p_{\mathrm{eqv}}}{\partial \boldsymbol{\varepsilon}^p} : \delta\boldsymbol{\varepsilon} \\ &= \left((1-\omega)\mathbf{E}^{\mathrm{epc}} - g'_{\mathrm{d}}(\varepsilon^p_{\mathrm{eqv}})\overline{\boldsymbol{\sigma}} \otimes \frac{\partial \varepsilon^p_{\mathrm{eqv}}}{\partial \boldsymbol{\varepsilon}^p} \right) : \delta\boldsymbol{\varepsilon} \\ &= \mathbf{E}^{\mathrm{epdc}} : \delta\boldsymbol{\varepsilon} \end{aligned} \tag{14}$$

where $\mathbf{E}^{\mathrm{epdc}}$ is the general form of elastoplastic-damage tangent modulus. In view of Equations (3) and (10), it can be written for the present model as

$$\mathbf{E}^{\mathrm{epdc}} = (1-\omega)\mathbf{E}^{\mathrm{epc}} - \frac{\omega_{\mathrm{c}}}{\varepsilon_{\mathrm{pR}} - \varepsilon_{\mathrm{pD}}} \sqrt{\frac{2}{3}} \overline{\boldsymbol{\sigma}} \otimes \frac{\boldsymbol{\varepsilon}^p}{\sqrt{\boldsymbol{\varepsilon}^p : \boldsymbol{\varepsilon}^p}} \tag{15}$$

When the equivalent plastic strain is smaller than the damage threshold value, $\varepsilon_{\mathrm{pD}}$, elastoplastic modulus $\mathbf{E}^{\mathrm{epc}}$ is valid. Beyond it, elastoplastic-damage modulus $\mathbf{E}^{\mathrm{epdc}}$ should be employed. During elastic loading and unloading, the damage elastic modulus, $(1-\omega)\mathbf{E}$, is used. Next, the present model is demonstrated with numerical simulations.

Numerical Examples

The present model response is demonstrated in uniaxial constitutive tests using a single element mesh depicted in Figure 3 with the material properties and model parameters. The governing field equations are discretized in time as well and then solved with the

implicit Newmark time integration scheme as sketched in Appendix A. The model is implemented in a self-written Matlab code.

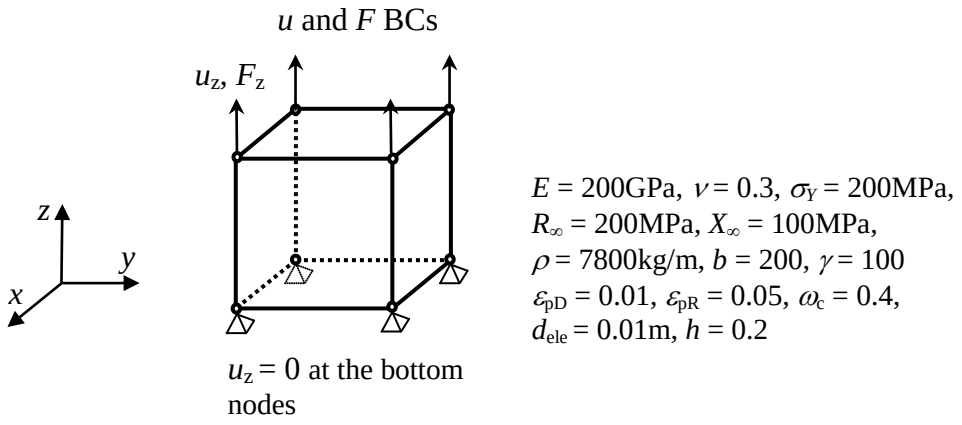

Figure 3. Single hexahedral element mesh and material properties.

The first example is a simulation of the 1D tension test due to a monotonically increasing loading applied to the nodes of the element as described in Figure 3. The loading sequence is divided in 388 time steps of equal lengths, 1 μs, and the maximum value of the loading is 2.7 times the yield load $\sigma_Y A_{ele}$ (= 20 kN). The results of the simulations are shown in Figure 4.

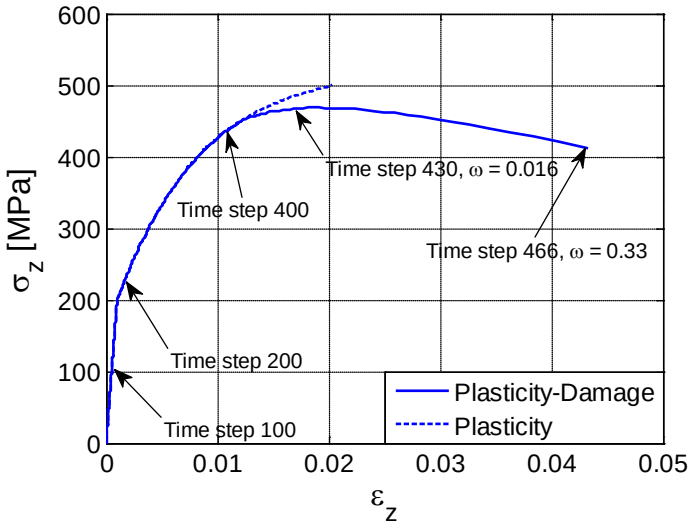

Figure 4. Simulated stress-strain response of the model in monotonic 1D tension test.

The effect of damage on the stress-strain response predicted with the model is crucial as it can be observed in Figure 4 where the results for the same test without the damage are plotted as well. The plain plasticity model goes on with the hardening needing ever

higher load level (until the saturation limit is reached R_∞) to increase the strain while the plasticity-damage model results in softening response and extensive straining in the loading direction.

In order to study the convergence properties of the model in global iteration, the error norms, i.e. the Euclidian norm of the residual, computed at the time steps indicated in Figure 4 are given in Table 1.

Table 1. Error norms for selected time steps in monotonic tension test.

Residual Norm $\|\mathbf{r}\|$, TOL = 1E−5					
Iteration/Time step	100	200	400	430	466
1	8.6341E+02	7.0232E+01	5.0926E+01	1.4920E+01	1.0664E+03
2	1.2248E−12	6.9354E+00	5.6437E−00	2.7747E−01	1.2517E+01
3		5.7291E−12	2.0099E−11	3.1421E−02	1.1051E+00
4				4.0591E−04	4.8147E−02
5				1.2600E−07	1.0234E−03
6					6.5272E−06

According to the residual norms in Table 1, the convergence rate is very high, especially before the onset of damaging. This convergence is due to the incrementally (in time steps) linear nature of the cutting plane algorithm. After the damage process is activated, the convergence rate is considerably slower. However, on decreasing the time step, the convergence is substantially accelerated. Indeed, when one tenth of the time step leading to convergence rates in Table 1 was used, the error norms given in Table 2 were obtained.

Table 2. Error norms for the last time step (4660) in tension test with reduced time step.

Iteration cycle	1	2	3	4
Residual Norm $\|\mathbf{r}\|$	7.9054E+01	6.2409E−03	4.1506E−06	3.3504E−10

This observation indicates that the tangent modulus (15) for the combined plasticity-damage model is algorithmically consistent. It should be noted that due to the predictor-corrector formulation of the solution scheme (see Appendix A) even the linear elastic loading (Time step 100 in Table 1) requires two steps to reach balance. Moreover, the hardening and damage parameters in Figure 3 are more or less randomly chosen and do not necessarily represent any real material.

The next (and final) test is a displacement (strain) driven cyclic loading in z-direction demonstrating the applicability of the model in low-cycle fatigue analyses. The sinusoidal loading programme is shown in Figure 5.

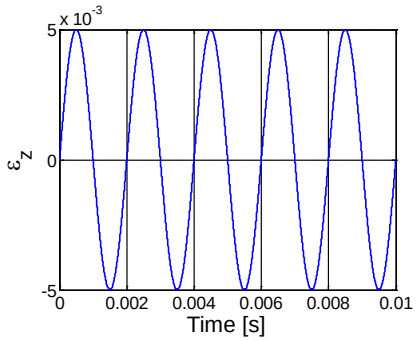

Figure 5. Sinusoidal cyclic strain BC for 1D tension-compression test.

The results of the simulation with the damage-plasticity model as presented above, pure plasticity model with nonlinear hardening laws (2), and pure plasticity model with linear isotropic and kinematic hardening are shown in Figure 6. The modulus for the linear isotropic and kinematic hardening is 0.1*E* (20 GPa).

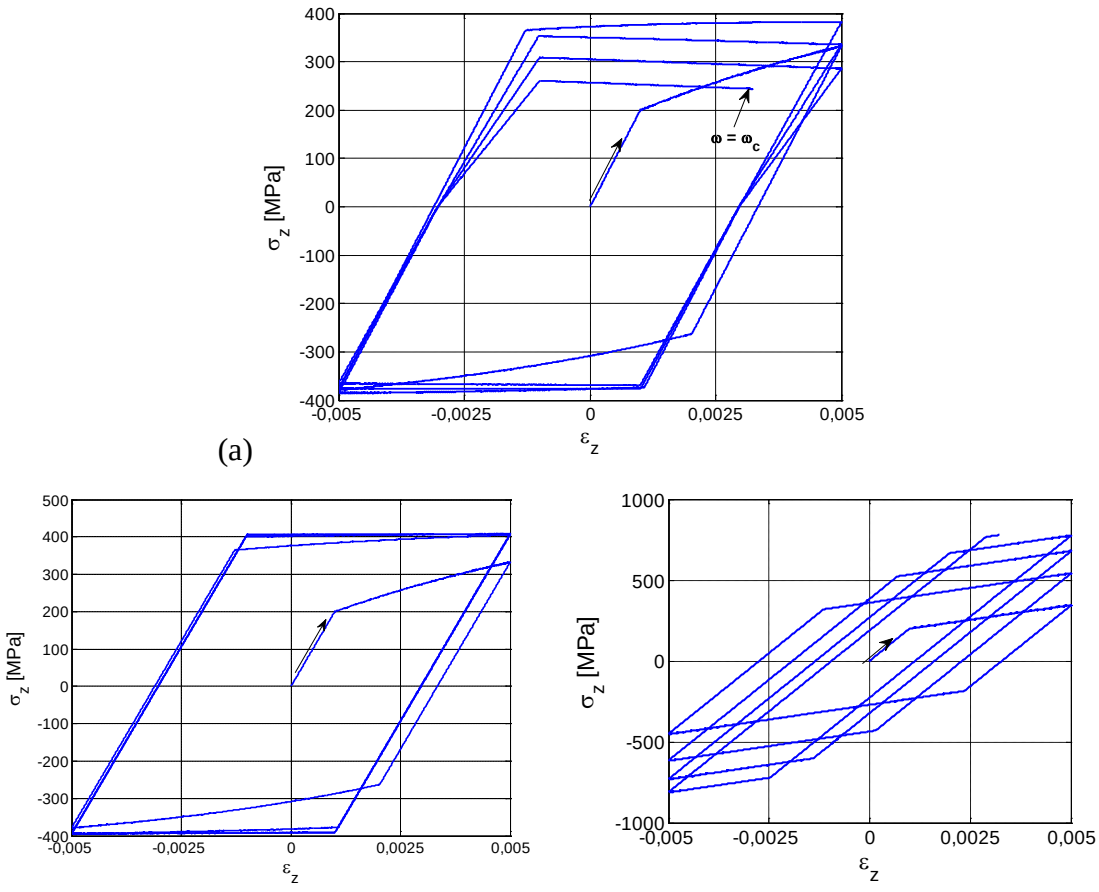

Figure 6. Simulated stress-strain response for 1D tension-compression test: Plasticity-damage model with nonlinear hardening laws (a), Plasticity model with nonlinear hardening laws (b), and Plasticity model with linear hardening laws (c).

The response in each case is quite different reflecting the importance of the model components for the adequacy of the simulated results. An ever increasing – and thus totally non-realistic – cyclic hardening behaviour is obtained with the linear hardening laws (Figure 6c). A substantially more realistic response is predicted with the non-linear hardening laws (see Figure 6b). The hardening behaviour saturates quickly after few cycles which is the realistic manifestation of hardening in general. However, the elastic loading and unloading takes place with the initial stiffness which is not realistic. Incorporation of the damage part of the model mends this deficiency by accommodating the stiffness degradation, as can be observed in Figure 6a. The microcrack closure effect (via relation (11)) can be clearly observed in Figure 6a as an asymmetry of the stress-strain response between tension and compression cycles. This is a real manifestation of many steels in low-cycle fatigue tests, see an example for AISI 316L stainless steel in [1]. Finally, the Bauschinger effect is observable in all the results in Figure 6.

Conclusions

The simple J_2-plasticity-damage model with nonlinear hardening laws presented in this paper can capture many of the salient features of metal behavior in low-cycle fatigue tests. These features include isotropic and kinematic hardening manifested as a rising yield strength and motion of the yield surface in the direction of plastic flow, strength degradation or softening, and stiffness degradation or damage. The features the model cannot capture are mostly those dictated by the small strain assumption and isotropic damage model. These include, e.g., the necking in uniaxial tension test up to the fracture and damage induced anisotropy.

The plasticity and damage parts were combined with the effective stress-space formulation resulting in a particularly simple and hence computationally cheap expression for the tangent stiffness matrix.

Acknowledgements

This work was financed by Finnish Academy (grant no. 251626).

Appendix A

Here the algorithm for solving the spatially (FE) discretized equations of motion of the boundary/initial value problem in time is presented for the convenience of the reader. The implicit Newmark time integration scheme is chosen for time discretization while Newton-Raphson method is employed in the iteration of materially nonlinear equation of motion

$$\begin{aligned} &\mathbf{M}\ddot{\mathbf{u}} + \mathbf{C}\dot{\mathbf{u}} + \mathbf{f}_{\text{int}} = \mathbf{f}_{\text{ext}} \quad \text{with} \\ &\mathbf{f}_{\text{int}} = \mathop{\mathbf{A}}_{e=1}^{n} \int_{V_e} \mathbf{B}_e^{\mathrm{T}} \boldsymbol{\sigma}_e \, dV_e \end{aligned} \tag{A1}$$

where **M** is the lumped mass matrix, **C** is the damping matrix (set to zero in this paper), **B** is the small deformation kinematic matrix, $\mathbf{f}_{\text{int}}$ and $\mathbf{f}_{\text{ext}}$ are the internal and external force vector, respectively, V_e is the element volume and, finally, **A** is the standard finite element assembly operator. The integration in (A1) is performed numerically in the Gaussian points.

Since the elemental stresses $\boldsymbol{\sigma}_e$ are obtained through the stress return mapping scheme, Equation (A1) is nonlinear (materially) and needs to be solved iteratively by using the Newton-Raphson method. For this end, the internal force vector (other terms are linear) needs to be linearized resulting in relation

$$\begin{aligned} d\mathbf{f}_{\text{int}} &= \mathop{\mathbf{A}}_{e=1}^{n} \int_{V_e} \mathbf{B}_e^{\mathrm{T}} \mathbf{E}_{\text{alg}} \mathbf{B}_e \, dV_e \, d\mathbf{u} \\ &= \mathbf{K}_{\tan} d\mathbf{u} \end{aligned} \tag{A2}$$

where Equation (14) and relation $\boldsymbol{\varepsilon} = \mathbf{B}\mathbf{u}$ have been used along with (A1), and $\mathbf{E}_{\text{alg}}$ denotes the algorithmic tangent modulus depending on the loading as explained earlier. $\mathbf{K}_{\tan}$ is the global tangent stiffness matrix.

The Newmark difference formulas are

$$\begin{aligned} \dot{\mathbf{u}}_{n+1} &= \dot{\mathbf{u}}_n + (1-\gamma)\Delta t \ddot{\mathbf{u}}_n + \gamma \Delta t \ddot{\mathbf{u}}_{n+1} \\ \mathbf{u}_{n+1} &= \mathbf{u}_n + \Delta t \dot{\mathbf{u}}_n + (\tfrac{1}{2} - \beta)\Delta t^2 \ddot{\mathbf{u}}_{n+1} \end{aligned} \tag{A3}$$

where Δt is the time step and γ, β are the parameters which, with values $\gamma = 0.5$, $\beta = 0.25$, give the method unconditional stability with respect to time step. Now the solution algorithm can be written as follows:

1. Calculate the predictors: $\ddot{\mathbf{u}}_{t+\Delta t}^{0} = \mathbf{0}$, $\dot{\mathbf{u}}_{t+\Delta t}^{0} = \dot{\mathbf{u}}_t^0 + (1-\gamma)\Delta t \ddot{\mathbf{u}}_t$, $\mathbf{u}_{t+\Delta t}^{0} = \mathbf{u}_t^0 + \Delta t \dot{\mathbf{u}}_t + (\tfrac{1}{2} - \beta)\Delta t^2 \ddot{\mathbf{u}}_t$. Set $k = 0$.
2. Perform the stress return mapping and damage update to obtain $\boldsymbol{\sigma}^k$.
3. Evaluate the residual: $\mathbf{r} = \mathbf{f}_{t+\Delta t}^{\text{ext}} - \mathbf{f}_{\text{int}}^{k}(\boldsymbol{\sigma}^k) - \mathbf{M}\ddot{\mathbf{u}}_{t+\Delta t}^{k}$
4. If $\|\mathbf{r}\| < TOL$ set $t = t + \Delta t$ and go to 1. Else go to 5.
5. Evaluate tangent stiffness matrix $\mathbf{K}_{\tan}^{\text{dyn}} = \mathbf{K}_{\tan} + \frac{1}{\beta \Delta t^2}\mathbf{M}$ and solve for $\Delta\mathbf{u}$ from equation $\mathbf{K}_{\tan}^{\text{dyn}} \Delta\mathbf{u} = \mathbf{r}$.
6. Correct the predictors: $\ddot{\mathbf{u}}_{t+\Delta t}^{k+1} = \ddot{\mathbf{u}}_{t+\Delta t}^{k} + \frac{1}{\beta \Delta t^2}\Delta\mathbf{u}$, $\dot{\mathbf{u}}_{t+\Delta t}^{k+1} = \dot{\mathbf{u}}_{t+\Delta t}^{k} + \frac{\gamma}{\beta \Delta t}\Delta\mathbf{u}$, $\mathbf{u}_{t+\Delta t}^{k+1} = \mathbf{u}_{t+\Delta t}^{k} + \Delta\mathbf{u}$. Set $k = k + 1$ and go to 2.

While zero-acceleration predictor has been used in Step 1 of the algorithm, other kind of predictors are possible as well.

References

[1] J. Lemaitre, *A Course on Damage Mechanics*, Springer-Verlag, 1990.

[2] E.A. de Souza Neto, D. Peric, D.R.J. Owen, *Computational Methods for Plasticity, Theory and Applications*, John Wiley & Sons, 2008.
[3] J.C. Simo, T.J.R. Hughes, *Computational Inelasticity*, Springer, 2000.
[4] P. Grassl, M. Jirásek, Damage-plastic model for concrete failure, *International Journal of Solids and Structures*, 43: 7166-7196, 2006.

Timo Saksala
Tampere University of Technology
Department of Mechanics and Design
P.O. Box 589, FI-33101, Tampere, Finland
timo.saksala@tut.fi